Roles of the Debye Length and Skin Depth in the Characterization of Space Charge Interactions in Semiconductor Nanoparticles

Zhijing Hu[1], Zi Wang[2], Yanlin Li[3], Tao Shen[4], Ming Yan[1], Thomas Wong[2,*]

[1]Keysight Technologies, Thousand Oaks, CA 91360, USA
[2]Department of Electrical and Computer Engineering, Illinois Institute of Technology, Chicago, IL 60616, USA
[3]Qorvo, Greensboro, NC 27409, USA
[4]College of Information Engineering and Automation, Kunming University of Science and Technology, Kunming, Yunnan 650093, China

*Corresponding author: E-mail: twong@ece.iit.edu

Non-degenerate semiconductor nanoparticles with bulk plasma frequency in the terahertz frequency range are of substantial current interest for device and sensing applications in that part of the electromagnetic spectrum. The penetration of electromagnetic field in a material containing mobile charges is governed by two length scales, namely the Debye length and the skin depth. Their relative influence on the response of a semiconductor nanoparticle to an external terahertz electric field is examined in this Letter. A transport-based formulation to describe charge-field interactions by coupling the Boltzmann equation with the field equations is employed to characterize space-charge effects. Numerical results computed with the charge transport formulation reveal that plasmonic interactions in a semiconductor nanoparticle remains a surface phenomenon up to the surface plasmon resonance frequency, beyond which it evolves into a bulk phenomenon as the inertia effect of the charge carriers subdues their response to the field, which penetrates deeper into the particle as the frequency is increased. Examination of the spectra of charge, field, and current distributions allows for the identification of the influence of particle size, Debye length and skin depth on space charge interactions in a semiconductor nanoparticle.

Introduction

Surface plasmon resonance in metallic nanoparticles (MNP) have led to numerous applications in sensing, waveguiding, and biomedical applications of MNPs and their derivatives. Owing to the bulk plasma frequencies of metals being in the optical region, activities of MNPs have been concentrated in that part of the spectrum [1-4]. With a lower charge concentration, hence a correspondingly lower bulk plasma frequency, semiconductor nanoparticles (SNPs) have attracted recent interest for device and component development in the terahertz and far infra-red frequency range [5-8]. Degenerately doped SNP can have plasma frequencies in the mid infra-red region, with properties similar to MNP [9-11]. While the response in non-degenerate SNPs is weaker than their metallic counterpart, SNPs can have their charge concentration varied by doping or otherwise, offering an additional degree of freedom in their design and preparation, leading to a wider range in properties. Polarization and plasmonic interactions in MNP have often been accounted for by dielectric functions based on the Drude model for electron dynamics in the optical region. Because the charge concentration in semiconductors are lower than that in metals, the electric field can penetrate deeper into a semiconductor. As a result, space charge can build up near the surface of an SNP, which cannot be accounted for by a bulk dielectric function as in the case of the MNP. To describe the accumulation and depletion of charges arising from the migration of electrons and holes in a semiconductor, transport formulation for carrier dynamics may be employed. This can be accomplished by coupling the Boltzmann equation with the equations for the electromagnetic field to obtain the collective response resulting from field-charge interactions.

A phenomenon accompanying space charge is its screening effect on the electric field that induces the formation of the space charge. The transport-based formulation enables a quantitative account of the charge and field distribution in the particle, leading to the determination of the induced dipole moment on the SNP, which is of fundamental importance in the characterization of the collective response of the SNP to a polarizing field. To gain physical insight to the nature of charge-field interaction, an examination of the evolution of the charge and field distributions in the SNP over a sufficiently broad spectrum can reveal the nature of the dynamics. In this Letter, spectral properties of parameters such as the Debye length and skin depth are studied for their influence on the charge and field distributions in an SNP, employing a charge-transport formulation. The discussion is

Advanced Materials Letters
www.vbripress.com/aml

IAAM®
Advancement of Materials to Global Excellence
www.iaamonline.org

concentrated on non-degenerate SNPs, for which space-charge effects are pronounced.

Charge carrier transport in semiconductor nanoparticles

Conventional approach to the characterization of polarization of a homogeneous small conductive spherical particle placed in a dynamic electric field in free space leads to an induced dipole moment given by

$$p = 4\pi\varepsilon_0 a^3 \frac{\varepsilon(\omega) - \varepsilon_0}{\varepsilon(\omega) + 2\varepsilon_0} E \qquad (1)$$

where a is the radius and $\varepsilon(\omega)$ is the complex permittivity (dielectric function) accounting for the dielectric response of the particle [12]. This equation is evolved from the response of a dielectric sphere to a static electric field. Its extension to the dynamic case is accomplished by replacing the dielectric constant with a frequency dependent dielectric function. By incorporating with the dielectric function the bulk conductivity given rise to by the conduction electrons, the equation can account for the surface plasmon resonance exhibited by metallic nanoparticles with a peak of the dipole moment in the optical region [13]. It also produces similar effects on the dipole moment in the terahertz and infra-red range for an extrinsic semiconductor nanoparticle. The surface plasmon resonance frequency ω_{ps} can be estimated from equation (1) by noting that $\varepsilon(\omega) + 2\varepsilon_0$ in the denominator would be at its minimum at the resonance, leading to

$$\omega_{ps} = \sqrt{\frac{Ne^2}{\varepsilon_0 m^*(\varepsilon_r + 2)}} \qquad (2)$$

where ω_{ps} is the surface plasmon frequency. In (2), N is the electron concentration at equilibrium and m^* is the effective mass of the charge carrier. A small damping due to carrier collision is assumed to justify the usage of this result. When $\varepsilon_r = 1$ as in the case of an electron gas, (2) gives

$$\omega_{ps} = \sqrt{\frac{Ne^2}{3\varepsilon_0 m^*}} = \frac{\omega_p}{\sqrt{3}} \qquad (3)$$

which has been employed to estimate ω_{ps} for MNP, where the response is dominated by the electrons, owing to the abundance.

For SNP, the polarization in the crystal lattice needs to be taken into consideration, and ε_r of the intrinsic semiconductor needs to be employed, which is usually considerably larger than 1, leading to an ω_{ps} that lies close to ω_p, the bulk plasma frequency.

However, a drawback of (1) is that it always gives a value of $4\pi\varepsilon_0 a^3 E_0$ in the static limit, which is the dipole moment for a perfectly conducting sphere in a static field. Even if the SNP has a low carrier concentration (low doping level), the dipole moment always reaches this value in the static limit. This is a consequence of using a bulk material parameter to account for response subject to surface effect.

This difficulty can be alleviated by introducing a transport formulation to account for the motion of the charge carriers so that the bulk conductivity is replaced by the concentration and velocity of the charge carriers, each being a dynamical variable coupled to the electric field [13, 14].

Since equation (1) originated from static consideration, it reflects mainly the effect of the shape of the sphere. Relying on the consideration of $\varepsilon(\omega) + 2\varepsilon_0$ to estimate ω_{ps} does not enable the size influence of the particle on the resonance frequency to be revealed, unless an effective value of ε_r tied to the radius is introduced. This can also be overcome by employing a transport formulation to characterize the motion of the mobile charge carriers. There are mainly three mechanisms related to particle size that can influence field-charge interactions in an SNP, namely quantum size effects, reduction in mean-free path of the charge carriers, and depth of field penetration. In this paper we are mainly interested in space-charge effects and will confine the discussion to SNPs with radius of 5 nm to 500 nm and doping range of 10^{16} cm^{-3} to 10^{20} cm^{-3}, for which the dominant size influence occurs when the depth of field penetration becomes comparable to the radius of the particle.

The equation of motion for conduction-band electrons in a doped SNP not far from thermal equilibrium can be written as [14].

$$\frac{\partial(n\mathbf{v}_n)}{\partial t} = -\frac{kT}{m_n^*}\nabla n - \frac{qn}{m_n^*}E - \frac{n\mathbf{v}_n}{\tau_n} \qquad (4)$$

$$\nabla \cdot \mathbf{J} = q\frac{\partial n}{\partial t} + qR_n \qquad (5)$$

In the equations, n, v_n, m_n^* and τ_n are the density, velocity, effective mass and momentum relaxation time for the electron respectively. R_n is the net recombination rate. T is the absolute temperature and k is the Boltzmann constant. The current density is given by

$$\mathbf{J}_n = -qn\mathbf{v}_n \qquad (6)$$

The electric field can be expressed in terms of a scalar potential, which is time dependent and satisfies the Poisson's equation for quasi-static consideration, is given by

$$\nabla^2\phi = \frac{q(n - N_e)}{\varepsilon_s} \quad \text{and} \quad E = -\nabla\phi \qquad (7)$$

N_e is the nominal electron concentration at equilibrium, given by the doping level. A similar set of equations can be written for the holes if the SNP is of p-type. Solving these coupled equations with appropriate boundary conditions leads to the distributions of electric field, charge density and current density in the SNP, in response to an originally uniform dynamic electric field in which the SNP is immersed. The polarization in the SNP gives rise to an exterior dipole field for which the dipole moment can be calculated by first principle integration of the charge distribution or estimated from the exterior field.
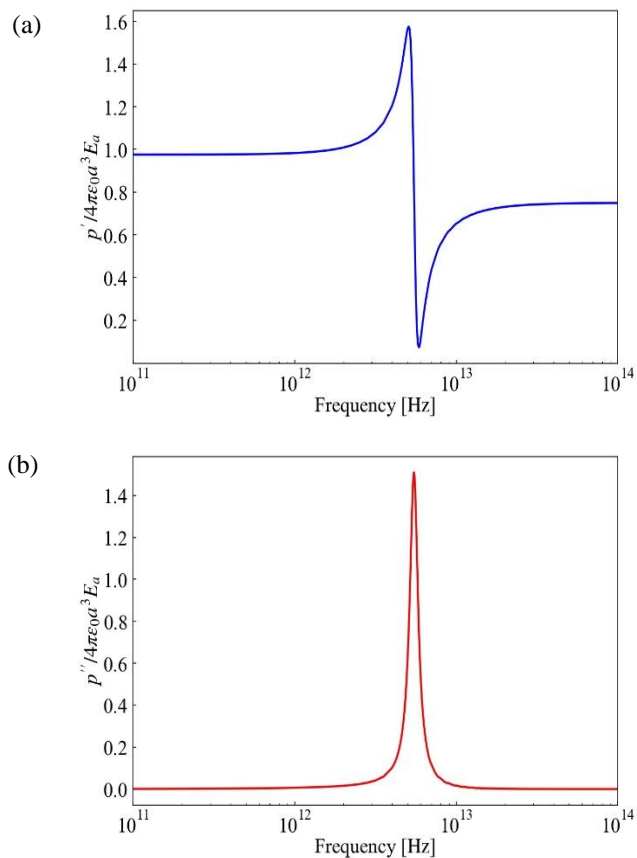
**Advanced
Materials Letters**
www.vbripress.com/aml

IAAM ®
Advancement of Materials
to Global Excellence

www.iaamonline.org

(a)

(b)

Fig. 1. Total induced dipole moment on a semiconductor nanoparticle vs. frequency. (a) Real part, (b) Imaginary part. The calculations are performed for particles with radius $a = 50$ nm, $\varepsilon_r = 10$, electron effective mass $m^* = 0.25m_o$ and momentum relaxation time $\tau_n = 2 \times 10^{-13}$ s.

Numerical solutions for the system of equations

The system of equations for the electric field intensity, charge density and charge velocity can be solved analytically as well as numerically using a simulation tool based on finite element method. Very good agreement between the two approaches were obtained. From the charge distribution and field intensity, the total induced dipole moment on the SNP, $p' - jp''$, can be computed. Alternatively the dipole moment can be estimated by noting the exterior field intensity, after establishing that the exterior field is a dipole field. Frequency dependence of the total dipole moment induced by the applied field on an SNP is shown in **Fig. 1**. In the low frequency range, the SNP acquires a polarization arising from accumulation of charges close to the surface of the particle, giving a real part of dipole moment, p', close to $4\pi\varepsilon_0 a^3 E_0$ and a negligible imaginary part, p''. In this region, the dipole moment is essentially in phase with the applied field, with little power dissipation. In the vicinity of the surface plasmon resonance (SPR), a strong dispersion in the real part is observed, which is accompanied by a peak in the imaginary part, accounting for the power absorption by the SNP. Beyond the SPR frequency, the imaginary part settles quickly to small values and approaches zero asymptotically, while the real part approaches a value given by the high-frequency

limit of (1), where the response is mainly contributed from the lattice polarization, since the conduction electrons cannot follow the rapidly changing field due to inertia effects. The SNP is acting as a dielectric particle, with a relativity permittivity of ε_r for the semiconductor when it is intrinsic. The dispersion effects of the polarization process give rise to a minimum in p' in a range of frequencies immediately above the SPR. If the SNP has a higher doping level such as 10^{19} cm^{-3}, p' in this region becomes negative. This response can be impetus for producing inductive reactance for terahertz circuitry.

The nature of the influence of particle size on SPR can be visualize by reviewing the charge distribution in the SNP below its bulk plasma frequency, as shown in **Fig. 2(a)** and **Fig. 2(b)**. It is calculated for the SNP with the dipole moment shown in Fig. 1. It can be seen that the charges accumulate in the regions close to the spherical surface. The charges have a shielding effect on the applied field, preventing it from reaching the interior of the SNP. At low frequencies, the penetration depth of the field is close to the Debye length, which accounts for the charge profile in the static limit. As the frequency is increased, deeper penetration will take place. Passing beyond the SPR, standing wave patterns are observed for both the charge density and the interior field of the SNP, while the exterior field still maintains a dipole pattern. Plasmonic interaction has evolved from a surface phenomenon at low frequencies to a bulk phenomenon after reaching ω_{ps}, as shown in **Fig. 2(c)** and **Fig. 2(d)**.
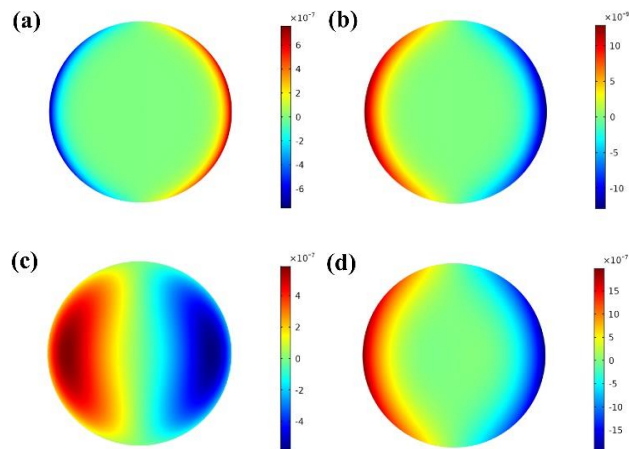

Fig. 2. Net charge in a semiconductor nanoparticle at doping of $N = 10^{18}$ cm^{-3} immersed in an originally uniform electric field of 1 V/cm. (a) Real part at frequency $f = 1$ THz. (b) Imaginary part at frequency $f = 1$ THz. (c) Real part at frequency $f = 5.68$ THz, near SPR freqneucy. (d) Imaginary part at frequency $f = 5.68$ THz, near SPR freqneucy.

When the radius of the particle is substantially larger than the Debye length, the interaction between the charge and the field is confined to the region close to the spherical surface of the particle. Change in the size of the particle does not have significant influence on the interior field beyond a few Debye lengths. Hence it is a surface

phenomenon so that ω_{ps} is not much affected by particle size. However, as the size of the particle is reduced to the range where the radius is comparable to the Debye length, screening effect of the charge will be affected and a blue shift of ω_{ps} will result. This is revealed in **Fig. 3**, in which topographical views of the variation in ω_{ps} with respect to changes in doping level and particle radius are displayed.
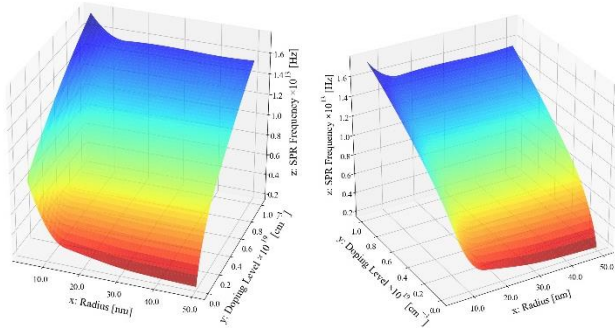

Fig. 3. Two perspectives of SPR frequency ($\omega_{ps}/2\pi$) topography as a function of doping level and particle radius, for the nanoparticle with material parameters same as those for Figure 1. Blue shift in ω_{ps} is observed for radius smaller than 10 nm.

While the Debye length is a good indication of the screening effect of charges on a static or low-frequency field, the penetration of an applied field into a semiconductor will generally increase when the excitation frequency is high. When it is beyond ω_{ps}, the inertia effect of the charge carrier prevents it from following the rapid variations in the field intensity, resulting in the weakening of the charge carriers' screening effect. There is considerable penetration of the field into the interior of the particle at higher frequencies, as seen in Figure 2c and 2d.

When the frequency is substantially higher than the SPR frequency, response from the electron motion are increasingly becoming weaker so that the polarization process is mainly contributed from the crystal lattice. The SNP appears essentially as a dielectric particle. A quantitative visualization of the charge distribution in the three regions of plasmonic interaction can be obtained by plotting the net charge density along a diameter of the particle aligned with the direction of the applied electric field, as shown in **Fig. 4**.

From the charge distributions in **Fig. 4**, it can be observed that the plasmonic response evolves from a surface phenomenon at low frequencies below the SPR to a bulk phenomenon at frequencies above it.

The presence of phase shift in the response along the diameter in the direction of the field is expected, since plasma waves are longitudinal, as net charge is present in the nanoparticle. However, a quasi-static formulation is adequate to account for most of the aspects of the field-charge interaction. The evolution in the charge distribution as the frequency is increased, depicted in **Fig. 4** can be understood by considering the equations governing the field and charge in the SNP.

In the static limit, the potential can be obtained from (7) with Boltzmann statistics for the electron density. Under weak field approximation, the potential satisfies a linearized equation given by

$$\nabla^2 \phi - \frac{1}{L_D^2} \phi = 0 \qquad (8)$$

where L_D, the Debye length, is

$$L_D = \sqrt{\frac{\varepsilon k T}{e^2 N_D}} \qquad (9)$$

which characterizes the screening effect of the static charge, extended to the lower frequencies [15]. Under a dynamic field, (4) through (7) solved together lead to a charge distribution given by [14]

$$\rho = -q A \left(\frac{\cosh(k_D r)}{k_D r} - \frac{\sinh(k_D r)}{k_D^2 r^2} \right) \cos\theta \qquad (10)$$

The electron density is characterized by

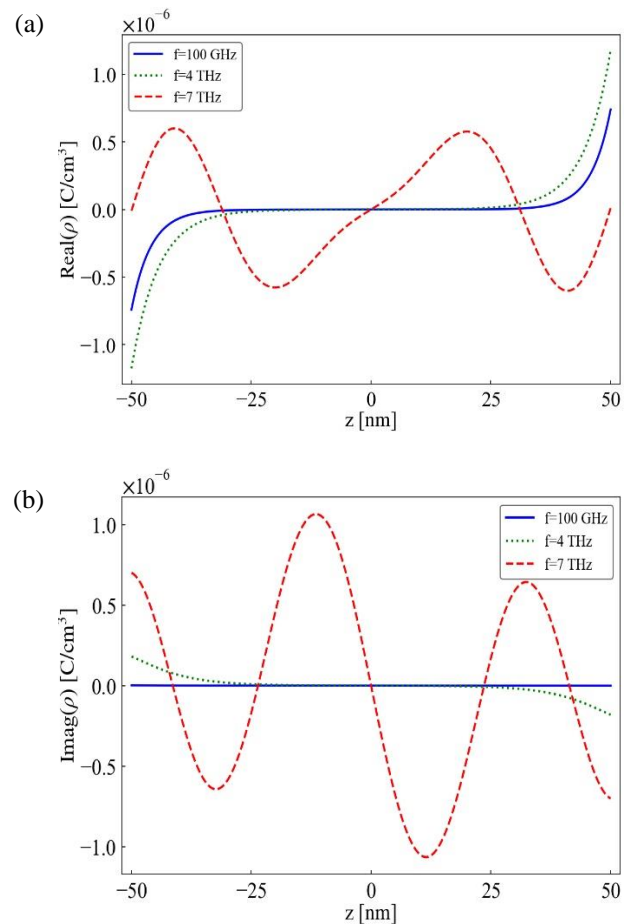$$\nabla^2 n - k_D^2 n = 0 \qquad (11)$$

Fig. 4. Net charge density along the diameter of the SNP parallel to the applied electric field at different frequencies. (a): real part. (b): imaginary part. Parameters for the nanoparticle are the same as those of the particle for Figure 1.
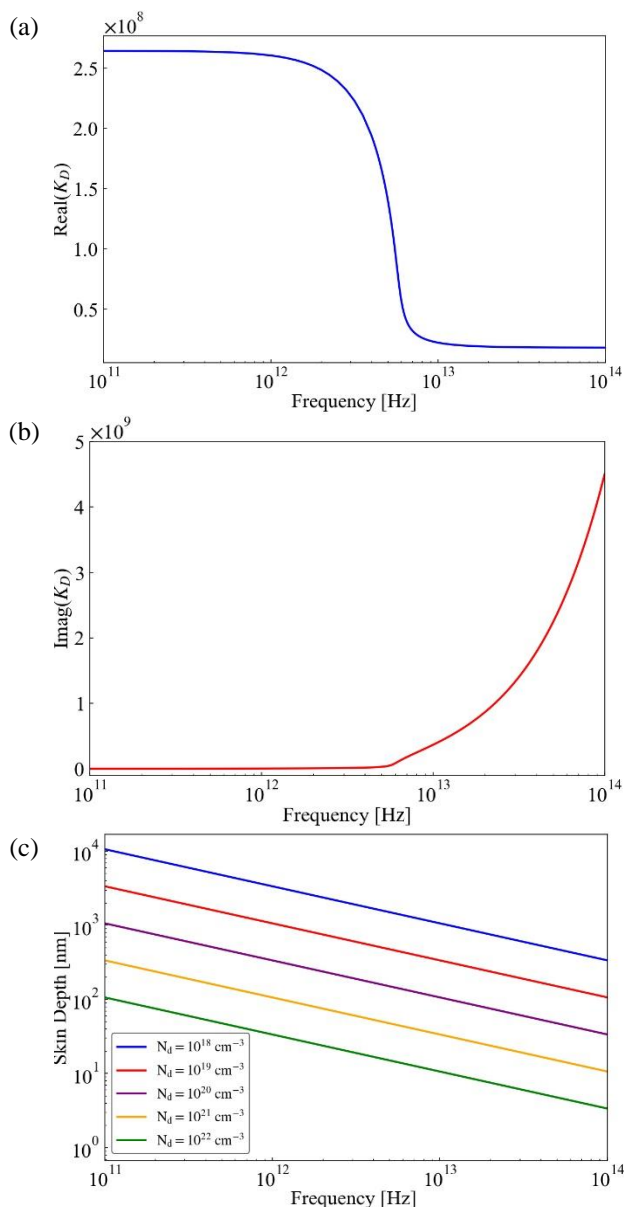
Fig. 5. (a) Real part of K_D, the wave number for the charge density, (b) Imaginary part of the wave number for the charge density, (c) skin depth as a function of frequency for different doping levels.

The frequency dependence of the complex wave number k_D in (11) that governs the charge distribution exhibits a frequency dependence which is shown in **Fig. 5(a)** and **Fig. 5(b)**. It has a real part that matches with the reciprocal of L_D in the static limit, with little variation until the SPR frequency is approached, while the imaginary part is negligible in the corresponding frequency range. This is consistent with the exponential decay in the charge distribution for the 0.1THz and 4THz response shown in Figure 4. As the frequency goes beyond that of the SPR, a reduction in the real part of k_D is seen, indicating smaller attenuation, hence deeper penetration of the field, reflecting a reduction in screening effect of the space charge, which is spread over a larger distance. Accompanying the reduction in decay of the charge and field profiles is the dispersion

effect as depicted by a gradual increase in the imaginary part of k_D as shown in **Fig. 6(b)**. At 7 THz there is considerable field penetration and dispersion effects so that a standing wave is built up in the SNP, as seen in **Fig. 4.** The plasmon interaction at this frequency has evolved to become a bulk phenomenon.

One may conclude from the consideration of the data shown in Figures 4 and 5 that plasmonic interaction in SNP is a surface phenomenon at low frequencies, up to the SPR. The charge and field distributions are essentially characterized by a real constant related to material parameters. It is identified by the real part of k_D, a wave number, whose reciprocal can be considered as an extension of the Debye length L_D, to the dynamic case, becoming a frequency dependent parameter to characterize the dynamic screening effect of the space charge. As expected from dispersion relations, the imaginary part of k_D shows a corresponding increase with frequency, depicting an increase in the phase shift of the space-charge wave at higher frequencies.

At frequencies substantially higher than the SPR frequency, the inertia effect of the mobile electrons prohibits them from responding to the applied field, rendering their effects to be negligible. In this frequency range, the real part of the dipole moment is contributed from the lattice polarization of the SNP, which is characterized by the permittivity of the intrinsic semiconductor. Lattice dynamics and response of core electrons in most semiconductors do not give rise to electromagnetic dispersion below the infra-red region. Hence most intrinsic semiconductors have a frequency independent permittivity at wavelengths larger than 1 μm [**16,17**]. A corresponding small value in the imaginary part of the dipole moment is observed. At this high frequency range of terahertz, the SNP acts as a dielectric particle.

Quasi-static formulation has been employed up to this point in the characterization of space charge interactions in an SNP, where the doping level is below 10^{20} cm^{-3}. The inadequacy of the quasi-static formulation is revealed when the doping is high so that skin effect becomes significant. Skin effects are revealed by considering the current distribution. At low to moderate doping, considerable current flow through the interior of the SNP, as depicted by the colour plot shown in **Fig. 6(a)**. This form of current distribution is also exhibited even at very high doping level of 10^{21} cm^{-3} if the quasi-static formulation (7) is employed to describe the electric field, given in terms of a scalar potential.

However, for a highly conductive object in a dynamic electric field at high frequencies, skin effect will lead to a current that stays near the surface of the object. This phenomenon is not predicted by the use of a quasi-static formulation, which cannot account for retardation of the field. Retardation in a wave is characterized by its propagation constant which reflects attenuation and dispersion of both the electric field and the magnetic field coupled to each other. It is therefore necessary to abandon the quasi-static formulation and employ a full-wave

analysis when the doping level is high. Although the Mie series solution is a full-wave solution of the Maxwell's equations and has been employed with immense success in the treatment of electromagnetic wave scattering by dielectric spheres from VLF to optical range, dynamical response of the material is entered to the wavenumber in the coefficients of each term in the series by a complex permittivity. To account for conduction current in a conductive sphere, the permittivity is augmented with a term related to the bulk conductivity, often based on the Drude model. In the basic form, the Mie series with bulk material parameters do not treat charge density and velocity as separate variables. In this study, the full set of Maxwell's equations are coupled with the transport equations of the charge carriers, for which the density and velocity are separate variables. By coupling the full set of Maxwell's equations with the current density following from Equations (4) – (6), the wave equation for the electric field in the SNP can be obtained as

$$\nabla^2 \boldsymbol{E} + k_s^2 \boldsymbol{E} = (j\omega D_{ne} - \frac{1}{\varepsilon_0 \varepsilon_r})e\nabla n \qquad (12)$$

where
$$k_s^2 = \omega^2 \mu_0 \varepsilon_0 \varepsilon_r - j\omega\mu_0 e^2 D_{ne} N \qquad (13)$$

$$D_{ne} = \frac{kT\tau_n}{m_n(1 + j\omega\tau_n)} \qquad (14)$$
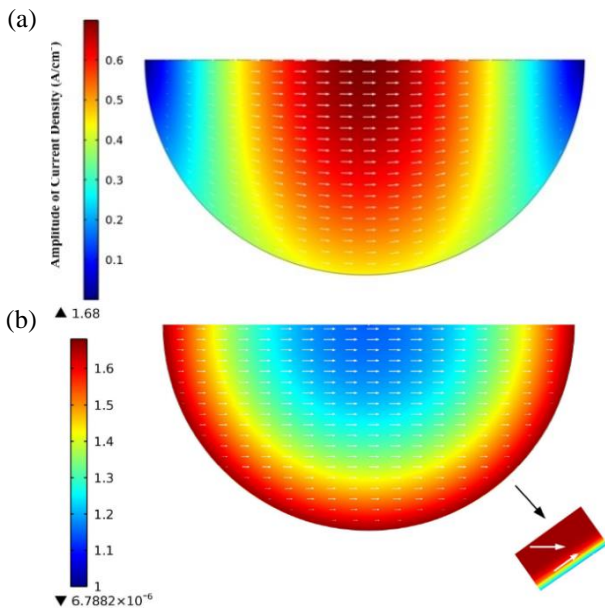
(a)

(b)

Fig. 6. Current distributions at 1 THz in an SNP. (a) Doping level is 10^{17} cm^{-3}, calculated by quasi-static or full-wave formulations (b) Doping level is 10^{22} cm^{-3}, calculated by full-wave formulation only.

Solving (12) with the boundary conditions for the field and current density at the surface of the SNP leads to the full-wave solution for the field, charge and current distributions. At low doping level, the full-wave solution gives the same current distribution as the quasi-static result shown in **Fig. 6(a)**. However, the full-wave solution gives a current distribution staying close to the surface of the particle for a highly doped SNP, as skin effect becomes

significant. A plot of the current distribution calculated from full-wave solution for a doping level of 10^{22} cm^{-3} is shown in **Fig. 6(b)**, which is vastly different from the one shown in Fig. 6(a). Although this represents the case of degenerate semiconductors, the display of the result of calculation is chosen to highlight the skin effect, which becomes more subtle at doping levels of 10^{21} cm^{-3} and below. We go beyond the range of doping level of main interest ($10^{16} – 10^{20}$ cm^{-3}) for display of data to enable skin effects to be conspicuous for ease of comparison.

While the screening effect of the net charge has influence for static and dynamic excitations, the skin effect is present only when a dynamic field is applied. Hence it is more pronounced at high frequencies. From the numerical computation viewpoint, it is of interest to know the threshold in the level of nominal charge concentration to require a full-wave formulation to realistically account for the field-charge interaction. This is largely determined by the magnitudes of the skin depth relative to the radius of the SNP and the Debye length.

When the former is much larger than the latter two as in the low to moderate levels of doping cases, quasi-static formulation will suffice. As the skin depth is reduced due to high carrier concentration as a result of doping, full-wave analysis is necessary to give a realistic account of the current distribution. A comparison of the variation in the skin depth, given by $(\sqrt{\pi f \mu \sigma})^{-1}$, with μ the permeability and σ the DC conductivity, as a function of frequency for different doping level is shown in Figure 5(c), which is calculated using the same material parameters as the nanoparticle shown in **Fig. 1**, except for the doping level. While a change in doping will inevitably result in change in other parameters such as the mean free path of the carriers and the relaxation time, for the purpose of comparison revealing the resultant increase in current flow as a consequence of nominal carrier concentration, the other parameters are held fixed so as to allow the effect of the primary parameter of interest to be revealed.

It can be observed from Figure 5(c) that for doping level of 10^{21} cm^{-3} and above, the skin depth at frequencies above 10 THz reduces to the 100 nm range. Hence crowding of the current to the surface of the particle becomes inevitable for a nanoparticle of 50 nm radius. At the same time, the reciprocal of the real part of k_D can also become comparable to the skin depth at high frequencies. In such cases, the interplay between space-charge and skin effects will jointly determine the dynamics of the charge and current distribution within the nanoparticle.

Conclusion

Surface plasmon resonance can be expected to enable semiconductor nanoparticles (SNPs) to be employed for sensors, circuitry and functional applications in the terahertz frequency range, in a role similar to that played by metallic nanoparticles in the optical range. An electromagnetic field penetrates into a semiconductor deeper than in a metal, leading to more significant space-

charge effects in an SNP compared to a metallic nanoparticle (MNP). To reveal space-charge distribution and field screening effects, a transport formulation for charge dynamics is employed to account for charge-field interactions. Analytical and numerical solutions are obtained for the system of equations derived by coupling the moments of the Boltzmann equation to the Maxwell's equations. Quasi-static formulation for the field is adequate for low to moderate carrier concentrations, but full-wave solution is needed when the skin depth is comparable to the radius of the particle or the Debye length. Below the surface plasmon resonance (SPR) frequency ω_{ps}, the space charge and the field stay close to the inner surface of the SNP, maintaining the response a surface phenomenon. The value of ω_{ps} is slightly smaller (less than 10% difference) than the bulk plasma frequency ω_p for SNP with radius in the 5 to 500 nm range when it is larger than the Debye length. A blue shift in ω_{ps} is displayed when the particle radius becomes comparable to or smaller than the Debye length. Beyond the SPR, screening effect of the space charge is reduced so that the response gradually evolves from a surface phenomenon to a bulk one, eventually giving rise to a standing wave. The reciprocal of the real part of the wave number for the net charge density converges to the Debye length in the static limit. It may therefore be considered as an extension of the Debye length for characterization of the dynamical screening effects of the space charge. At frequencies substantially above the SPR, space-charge response diminishes as a result of the inertia effect of the charge carriers. The SNP displays a high frequency response essentially that of a dielectric nanoparticle when space charge effects subside and interband transitions are absent, with a dipole moment determined by its high-frequency permittivity. For an SNP with high doping level in excess of 10^{20} cm^{-3}, full-wave solution of the field equations is needed to properly account for the current flow in the SNP as skin effects become prominent at high frequencies.

Supporting information

Supporting informations are available online at journal website.

Conflicts of interest
There are no conflicts to declare.

References

1. Barnes, W. L.; Dereux, A.; Ebbesen, T. W.; *Nature*, **2003**, *424*, 824.
2. Elghanian, R.; Storhoff, J. J.; Mucic, R. C.; Letsinger, R. L.; Mirkin, C. A.; *Science*, **1997**, *277*, 1078.
3. Lee, K.; El-Sayed, M. A.; *J. Phys. Chem. B*, **2006**, *110*, 19220.
4. Anker, J. N.; Hall, W. P.; Lyandres, O.; Shah, N. C.; Zhao, J.; Van Duyne, R. P.; *Nature Mater.*, **2008**, *7*, 442.
5. Yu, N.; Wang, Q.; Kats, M.; Fan, J.; Capasso, F.; Khanna, S.; Li, L.; Davies, A.; Linfield, E.; *Electron. Lett.*, **2010**, *46*, s52.
6. Lo, S.; Murphy, T.; *Appl. Phys. Lett.*, **2010**, *96*, 201104.
7. Kramer, N, J.; Schramke, K. S.; Kortshagen, U., R.; *Nano Lett.*, **2015**, *15*, 5597.
8. Pi, X.; Ni, Z.; Ding, Y.; Jiang, Y.; Jin, C.; Delerue, C.; Yang, D.; Nozaki, T.; *ACS Nano*, **2015**, *9*, 378.
9. Agrawal, A.; Johns, R. W.; Milliron, D.; *Annu. Rev. Mater. Res.*, **2017**, *47*, 1.
10. Kriegel, I.; Scotognella, F.; Manna, L.; *Phys. Rep.*, **2017**, *674*, 1.
11. Coughlan, C.; Ibáñez, M.; Dobrozhan, O.; Singh, A.; Cabot, A.; Ryan, K. M.; *Chem. Rev.*, **2017**, *117*, 5865.
12. Kerker, M.; The Scattering of Light and Other Electromagnetic Radiation. Academic Press, New York, **1969**.
13. Yan, M.; Wong, T.; *Proc. IEEE AP-S Int. Symp.*, **2006**, 935.
14. Shen, T.; Yan, M.; Wong, T.; *IEEE Trans. Antennas and Propag.* **2013**, *61*, 4229.
15. Hu, Z.; Shen, T.; Yan, M.; Wong, T.; *Proc. PIERS*, **2016**.
16. Yoo, H; Fauchet, P.; *Phys. Rev.*, **2008**, *B77*, 115355.
17. Green, M.; *Solar Energy Materials and Solar Cells*, **2008**, *92*, 1305.

Authors biography

Zhijing Hu received her bachelor's degree in electrical engineering from Xi`an Jiaotong University, and her M.S. and Ph.D. degrees in electrical engineering from Illinois Institute of Technology. Her study during school was focused on electromagnetics and semiconductor in THz domain. After graduation she has been working at Keysight Technologies and focuses on developing EDA tools

Zi Wang received his B.S. degree in communication engineering from Shandong University of Technology, Shandong, China in 2009 and his M.S. degree in electrical and computer engineering from Illinois Institute of Technology (IIT), Illinois, USA in 2013. Currently he is working on his Ph.D. in electrical engineering at IIT. His research interests include space-charge interactions in nanostructures and terahertz wave detection.

Yanlin Li received the B.S. degree from Huazhong University of Science and Technology, Wuhan, China, in 2011, and the M.S. and the Ph.D. degrees from Illinois Institute of Technology, Chicago, IL, USA, in 2013 and 2018, respectively. In 2018, she joined Qorvo, where she is currently an R&D Design Engineer with the Advanced Development Technology Platform.

Tao Shen, Ph.D., Professor, Deputy Dean of the College of Information Engineering and Automation, Kunming University of Science and Technology. He received the M.S. and Ph.D. degrees from Illinois Institute of Technology, USA in 2008 and 2013 respectively. Dr. Shen is the Deputy Secretary General of the Youth Work Committee of the China Material Research Society, member of IEEE and CCF. He has published more than 50 papers, 1 book and received 11 patents. His current research interests include intelligent detection and sensing, artificial intelligence and energy internet.

Ming Yan is an Expert Engineer in Keysight Technologies. He received his Ph.D. degree in electrical engineering from Illinois Institute of Technology in 2005. After his graduation, he joined Agilent/Keysight Technologies, where he works as an R&D engineer to develop RF/ Signal Integrity simulation technologies for the EDA software ADS.

Thomas Wong studied electrical engineering at the University of Hong Kong and did postgraduate research in microwave measurement of materials at Northwestern University. In 1981 he joined the Illinois Institute of Technology, where he is currently a Professor. His research has mainly been in applied electromagnetics, microwave instrumentation, and materials characterization. He has previously served as Department Chairman and Chair of Faculty Council. He is the author of *Fundamentals of Distributed Amplification* (Artech, 1993) and co-author of *Electromagnetic Fields and Waves* (Higher Education Press, 2006 & 2012).

Graphical abstract

On top is the frequency dependence of the real part of the induced dipole moment on a semiconductor nanoparticle displaying a surface plasmon resonance at 5.47 THz. Circular inserts are the color plots of net charge distributions in the nanoparticle below and above resonance. The topographical view displayed at the bottom depicts the variation of the surface plasmon resonance frequency as a function of particle radius and doping level.